

A comparison of the decomposition of electronically excited nitro-containing molecules with energetic moieties C–NO₂, N–NO₂, and O–NO₂

Atanu Bhattacharya, Yuanqing Guo, and Elliot R. Bernstein

Citation: *The Journal of Chemical Physics* **136**, 024321 (2012); doi: 10.1063/1.3668139

View online: <http://dx.doi.org/10.1063/1.3668139>

View Table of Contents: <http://aip.scitation.org/toc/jcp/136/2>

Published by the *American Institute of Physics*

COMPLETELY

REDESIGNED!



**PHYSICS
TODAY**

Physics Today Buyer's Guide
Search with a purpose.

A comparison of the decomposition of electronically excited nitro-containing molecules with energetic moieties C–NO₂, N–NO₂, and O–NO₂

Atanu Bhattacharya,^{a)} Yuanqing Guo, and Elliot R. Bernstein^{b)}

Department of Chemistry, Colorado State University, Fort Collins, Colorado 80523-1872, USA

(Received 4 September 2011; accepted 17 November 2011; published online 13 January 2012)

Decomposition of electronically excited nitro-containing molecules with different X–NO₂ (X = C, N, O) moieties has been intensively investigated over the past decades; however, their decomposition behavior has not previously been compared and contrasted. Comparison of their unimolecular decomposition behavior is important for the understanding of the reactivity differences among electronically excited nitro-containing molecules with different X–NO₂ (X = C, N, O) bond connections. Nitromethane (NM), dimethylnitramine (DMNA), and isopropylnitrate (IPN) are used as model molecules for C–NO₂, N–NO₂, and O–NO₂ active moieties, respectively. Ultraviolet lasers at different wavelengths, such as 226, 236, and 193 nm, have been employed to prepare the excited states of these molecules. The decomposition products are then detected by resonance enhanced two photon ionization (R2PI), laser induced fluorescence (LIF) techniques, or single photon ionization at 10.5 eV. NO molecules are observed to be the major decomposition product from electronically excited NM, DMNA, IPN using R2PI techniques. The NO products from decomposition of electronically excited (226 and 236 nm) NM and IPN display similar rotational (600 K) and vibrational distributions [both (0–0) and (0–1) bands of the NO molecule are observed]. The NO product from DMNA shows rotational (120 K) and vibrational distributions (only (0–0) transition is observed) colder than those of NM and IPN. At the 193 nm excitation, electronically excited NO₂ products are observed from NM and IPN via fluorescence detection, while no electronically excited NO₂ products are observed from DMNA. Additionally, the OH radical is observed as a minor dissociation product from all three compounds. The major decomposition pathway of electronically excited NM and IPN involves fission of the X–NO₂ bond to form electronically excited NO₂ product, which further dissociates to generate NO. The production of NO molecules from electronically excited DMNA is proposed to go through a nitro–nitrite isomerization pathway. Theoretical calculations show that a nitro–nitrite isomerization for DMNA occurs on the S₁ surface following a (S₂/S₁)_{CI} conical intersection (CI), whereas NO₂ elimination occurs on the S₁ surface following the (S₂/S₁)_{CI} conical intersection for NM and IPN. The present work provides insights for the understanding of the initiation of the decomposition of electronically excited X–NO₂ energetic systems. The presence of conical intersections along the reaction coordinate plays an important role in the detailed mechanism for the decomposition of these energetic systems. © 2012 American Institute of Physics. [doi:10.1063/1.3668139]

I. INTRODUCTION

Nitro-containing energetic materials such as TNT (2,4,6-trinitrotoluene), RDX (1,3,5-trinitro-1,3,5-triazacyclohexane), and PETN (2,2-bis-[(nitrooxy)methyl]-1,3-propanediol dinitrate or [3-Nitrooxy-2,2-bis(nitrooxymethyl)propyl] nitrate) have broad application as military explosives, propellants, and fuels. The molecular structures of these materials are illustrated in Fig. 1(a). The nitro (NO₂) functional group in these compounds is bonded to either carbon, nitrogen, or oxygen atoms. The different X–NO₂ (X = C, N, O) energetic moieties in nitroaromatic/nitroalkane, nitramine, and nitrate/nitroester

systems lead to unique and different energetic behavior among these materials. With regard to the sensitivity, in general, nitramines are more sensitive to shock or impact than nitroaromatics, and nitro esters are the most sensitive compounds of the X–NO₂ species.

Electronic excitations play important roles in the initial steps of the decomposition of these nitro-containing energetic materials.^{1–4} Due to the ultrafast⁵ and extremely exothermic nature of the decomposition of electronically excited large energetic materials, direct experimental elucidation of the initial steps of this process poses considerable challenge. Therefore, model systems, which are structurally similar to, but have fewer X–NO₂ energetic moieties than energetic materials, have been studied extensively^{6,7} to help establish the reaction pathways. In this regard, such model systems have been a primary focus for the study of the initial steps of the decomposition of their corresponding energetic systems. Moreover,

^{a)}Present address: Chemistry Department, Brookhaven National Laboratory, Upton, New York 11973, USA.

^{b)}Author to whom correspondence should be addressed. Electronic mail: erb@lamar.colostate.edu.

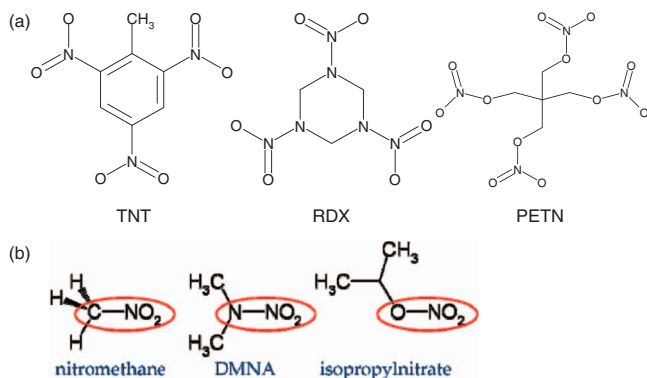


FIG. 1. Structures of $X\text{-NO}_2$ ($X = \text{C}, \text{N}, \text{O}$) containing energetic materials (a) and their model systems (b).

non-energetic model systems, such as nitromethane (NM), dimethylnitramine (DMNA), and isopropyl nitrate (IPN), represent baselines from which to evaluate the dynamics and mechanisms for the release of chemically stored energy from true energetic molecules. For instance, nitromethane has been studied as a model system for nitroalkanes with C-NO_2 moiety,⁶ dimethylnitramine has been studied as a model system for nitramines with the N-NO_2 moiety,⁷ and isopropyl nitrate has been studied as a good model system for PETN with the O-NO_2 moiety. The molecular structures of these model systems are illustrated in Fig. 1(b).

Details of the decomposition of electronically excited NM and DMNA have been presented in two of our recent publications.^{6,7} Nitro-nitrite isomerization followed by elimination of the NO molecule is found to be the major decomposition channel for electronically excited DMNA with a minor contribution from HONO elimination. Fission of the C-N bond to produce excited state NO_2 is found to be the major decomposition channel for electronically excited NM with minor contributions from both O elimination and HONO elimination. A certain degree of temperature and pressure dependence has also been observed from the decomposition of these two molecules in their excited electronic states.

As a model system for energetic materials with an O-NO_2 moiety, IPN has received much less attention than NM and DMNA, especially so with regard to the decomposition of electronically excited IPN. Several photodissociation pathways for alkyl nitrates have been proposed;⁸ however, analysis of internal (rovibrational) energy distributions of the decomposition product NO from IPN has not been studied thus far. Therefore, the study of decomposition of electronically excited IPN is an important part of the present work, in addition to the comparison of the decomposition behavior among the electronically excited molecules with C-NO_2 , N-NO_2 , and O-NO_2 active moieties. By comparing the decomposition behavior of electronically excited NM, DMNA, and IPN, we expect to obtain a better understanding of the initiation, sensitivity, kinetics, and dynamics of decomposition of different nitro-containing energetic materials. In addition, a comprehensive interpretation of the decomposition pathway through potential energy surface calculation will provide important insights into the effect of different $X\text{-NO}_2$ ($X = \text{C}, \text{N}, \text{O}$) bond connectivity on energetic systems.

II. EXPERIMENTAL AND THEORETICAL PROCEDURES

Detailed experimental procedures for study of the decomposition of NM and DMNA from excited electronic states have been described in our previous publications.^{6,7} Similar procedures have been employed to study the decomposition of IPN from its excited electronic states. In brief, the experimental setup consists of ns laser systems, a supersonic jet expansion pulsed nozzle, and two vacuum chambers: a time of flight mass spectrometer (TOFMS) chamber and an LIF (laser induced fluorescence) chamber. Excitation of sample molecules occurs at the excitation/ionization region of the spectrometers under collisionless conditions after molecular beam expansion. A single laser beam at 226 or 236 nm in the excitation/ionization region of the TOFMS is used to initiate decomposition of IPN, and to detect the NO product following a one-color (1+1) resonance enhanced two photon ionization (R2PI) scheme [$A^2\Sigma^+ (v' = 0) \leftarrow X^2\Pi (v'' = 0, 1)$, and $I \leftarrow A$ transition] through TOFMS. The UV laser wavelengths used in the R2PI experiments are generated by a pulsed dye laser, pumped by the second harmonic (532 nm) of a Nd:YAG laser's fundamental output (1.064 μm), in conjunction with a nonlinear wavelength extension system. Typical pulse energy of the UV laser is kept $\sim 16 \mu\text{J/pulse}$, which gives a laser beam intensity (I) $\sim 6.5 \times 10^6 \text{ W/cm}^2$ for an 8 ns pulse duration at a focused beam diameter of 0.2 mm. This low pulse energy goes not induce multiphoton dissociation of the parent molecules.

For the detection of an OH product from IPN through LIF, a UV laser at 226 nm is used to initiate the dissociation of the parent molecules and one additional laser (308 nm) is required to excite the OH $A^2\Sigma^+(v' = 0) \leftarrow X^2\Pi(v'' = 0)$ transition. Detection of the OH product from IPN has been precalibrated by the observation of the OH radical generated by photolysis of nitric acid (HNO_3) at 193 nm inside a quartz capillary attached to the pulse nozzle. Decomposition products of IPN are also detected in time-of-flight mass spectrometer by 118 nm ionization. An ArF excimer laser is used to generate radiation at 193 nm and the ninth harmonic (118 nm) of a seeded Nd:YAG laser is generated in a 1:10 mixture of Xe/Ar at 330 Torr pressure.

Isolated gas phase IPN molecules are generated through a supersonic jet expansion. The nozzle employed for the sample beam generation is constructed from a Jordan Co. pulsed valve. IPN is placed in a glass vial outside the nozzle and brought into the molecular beam by helium carrier gas at 30 psig backing pressure. This condition results in no cluster formation and a rotational temperature for molecules in the beam of less than 5 K.

The experiment is run at a repetition rate of 10 Hz. The timing sequence for the pulsed nozzle, and ionization laser is controlled by a time delay generator (SRS DG535). The molecular beam is perpendicularly crossed by a UV laser beam that is focused to a spot size of about 0.2 mm at the ionization region of a time of flight mass spectrometer. A background pressure of 1×10^{-5} Torr is maintained in the vacuum chamber during the experiment. Ions are detected by a microchannel plate detector (MCP) and fluorescence is

detected by a photomultiplier tube (PMT). Signals are recorded and processed on a PC using a box car averager (SRS SR 250) and an ADC card (Analog Devices RTI-800).

Theoretical results for NM are derived from Soto and co-worker's work.⁹ Detailed complete active space self-consistent field (CASSCF) calculation procedures for DMNA have been described in our previous publication.⁷ All geometry optimizations relevant to excited electronic state decomposition of IPN are performed at the CASSCF(10,7)/6-31G(d) level of theory with the GAUSSIAN 03 program.¹⁰ Orbitals used in the (10,7) active space are localized on O–NO₂ moiety. They include one NO bonding orbital σ_{NO} (in NO₂ moiety) one NO antibonding orbital σ_{NO}^* (in NO₂ moiety), one delocalized ONO π -bonding orbital π_{ONO} , one delocalized ONO π -antibonding orbital π_{ONO}^* , one π -nonbonding orbital $n\pi_{\text{O}}$, one σ nonbonding $n\sigma_{\text{O}}$, and one NO bonding orbital σ_{NO} (in O–NO₂ moiety). Similar active orbitals are also used for DMNA.⁷ Potential energy surfaces of electronically excited IPN are explored using both PES scans and an intrinsic reaction coordinate algorithm. Search of relevant conical intersections of IPN is performed using the algorithm implemented in GAUSSIAN 03 (Ref. 10). Vertical excitation energies are calculated by state-averaging over the ground and excited states with equal weights for each state; however, the state averaged wave function is not used to explore excited state PESs of IPN.

III. EXPERIMENTAL RESULTS

The decomposition of electronically excited NM, DMNA, and IPN is investigated and compared using a photodissociation/fragment detection (PD/FD) technique. In these cases, the gas phase parent molecules are excited through the absorption of a single UV photon and dissociation products are subsequently detected either by the same laser or a different time delayed laser through TOFMS or LIF spectroscopy. Photodissociation of NM, DMNA, and IPN following electronic excitation can potentially occur through different dissociation mechanisms on different electronic potential energy surfaces: NO₂ elimination, nitro-nitrite isomerization, O elimination, and HONO elimination. In order to determine critically which dissociation channel is open upon electronic excitation at 226, 236, and 193 nm, different ns laser experiments are performed. Results are presented and compared below.

A. NO₂ elimination channel and observation of NO

At 226, 236, and 193 nm excitations, the primary decomposition channel for NM is suggested to be NO₂ elimination⁶ producing electronically excited state NO₂ (1^2B_2). For DMNA with the same excitation conditions, the open decomposition channel is nitro-nitrite isomerization,⁷ producing electronically excited dimethylaminonitrite. The electronically excited NO₂ (1^2B_2) intermediate from NM and the dimethylaminonitrite from DMNA further dissociate into ground state NO (X), which is observed as a major decomposition product from NM and DMNA at 226 and 236 nm excitations. An NO product is also observed from the decomposition of IPN following electronic excitation at 226 and 236 nm.

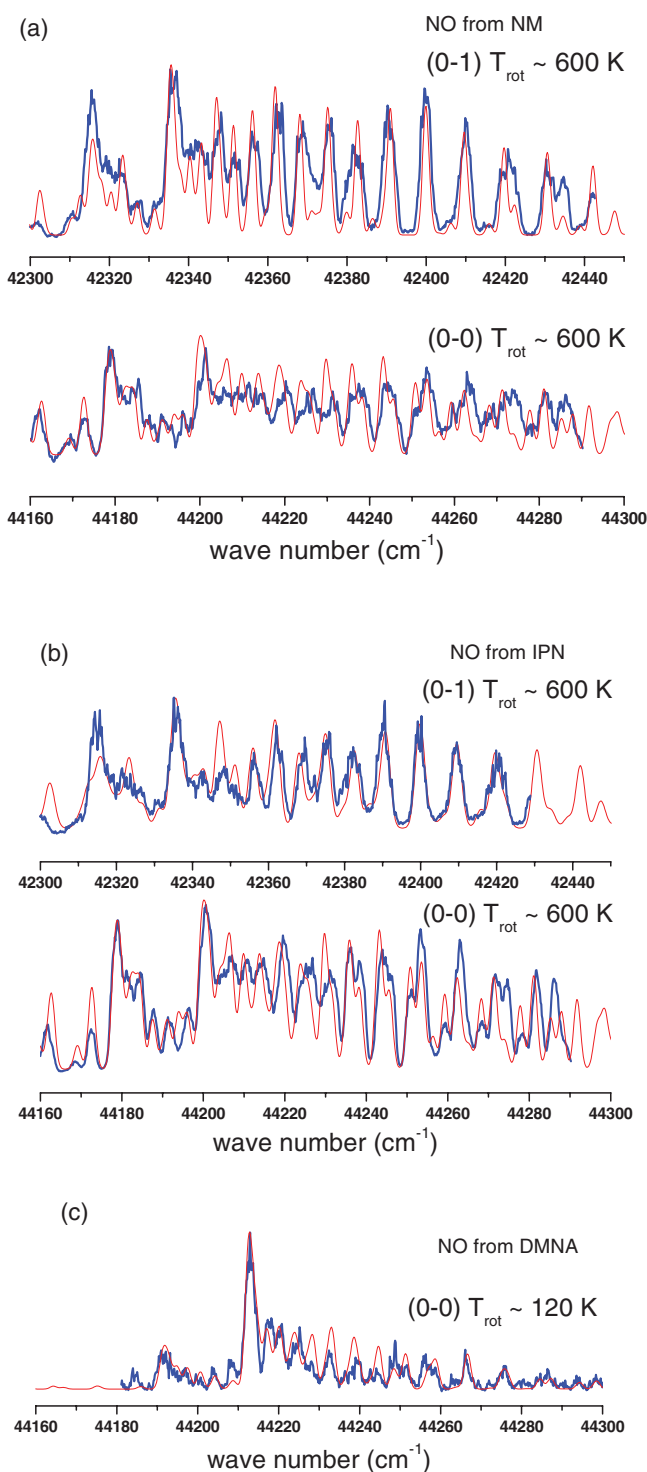


FIG. 2. One color (1+1) R2PI spectra of the vibronic transitions of the NO product from excited electronic state decomposition of (a) NM (C–NO₂), (b) IPN (O–NO₂), and (c) DMNA (N–NO₂). Rotational temperature simulations with Boltzmann distributions show that NO from NM and IPN generates rotational temperatures ~ 600 K; however, NO from DMNA renders a rotational temperature ~ 120 K.

The (1+1) REMPI spectra of the NO product from decomposition of electronically excited NM, DMNA, and IPN, in the NO $\text{A}^2\Sigma^+(v' = 0) \leftarrow \text{X}^2\Pi(v'' = 0, 1)$ transition region are shown in Fig. 2. The 226 and 236 nm excitation wavelengths, which are used to dissociate the parent

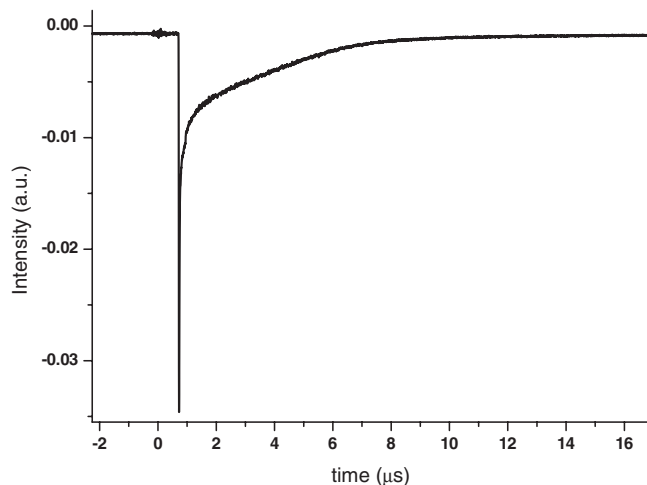


FIG. 3. NO_2 fluorescence emission observed following decomposition of IPN at 193 nm. Note that the observed lifetime of excited state NO_2 is $\sim 4 \mu\text{s}$. See text for details.

molecules, also correspond to the resonance (0–0) and (0–1) vibronic bands of the $A^2\Sigma(v' = 0) \leftarrow X^2\Pi(v'' = 0, 1)$ electronic transition of the NO product. Thereby, scanning the laser wavelengths, a (1+1) R2PI rotationally resolved spectrum of the NO product is obtained from photodissociation of NM, DMNA, and IPN. All the spectra are obtained under similar experimental conditions such as laser energy (50 $\mu\text{J}/\text{pulse}$), backing pressure (30 psig), and collisionless molecular beam conditions. Comparison of simulated spectra based on a Boltzmann population distribution for the NO product rotational energy levels at the $v'' = 0$ state yields a rotational temperature of $\sim 600 \text{ K}$ for both NM and IPN, and $\sim 120 \text{ K}$ for DMNA. Therefore, two vibrational bands ((0–0) and (0–1)) of the NO product from both NM and IPN are observed with similar rotational (600 K) distributions; however, only (0–0) transition of the NO product from DMNA is observed with the colder rotational (120 K) distribution. Based on this significant difference in rotational and vibrational distributions of the NO product from X– NO_2 (X = C, N, O) containing molecules, one can conclude that the decomposition behavior of the N– NO_2 active moiety is different from that of either C– NO_2 or O– NO_2 active moiety.

Additional decomposition behavioral similarities can be identified for NM and IPN. NO_2 elimination producing an electronically excited NO_2 intermediate (1^2B_2) as the primary channel for the decomposition of electronically excited NM is also confirmed by fluorescence from the NO_2 (1^2B_2) intermediate following photoexcitation of NM at 193 nm.^{6,11} Similar fluorescence in the visible region is also observed following IPN photodissociation at 193 nm, which is shown in Fig. 3. An excited state NO_2 fluorescence lifetime of $\sim 4 \mu\text{s}$ is observed. The actual lifetime for this NO_2 fluorescence is $\sim 32 \mu\text{s}$, however. The short life time of excited state NO_2 is observed probably due to the molecular beam longitudinal velocity ($\sim 2000 \text{ m/s}$) and the short ($< 2 \text{ cm}$) detection range for fluorescence. Within $\sim 4 \mu\text{s}$, excited NO_2 molecules escape from the fluorescence collection region.

In contrast, no NO_2 (1^2B_2) fluorescence is observed from DMNA at 193 nm excitation. Thereby, excited state NO_2 is

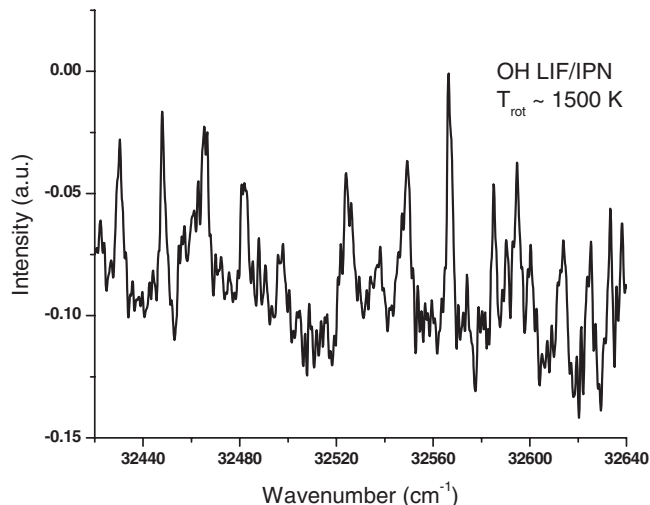


FIG. 4. LIF spectrum of OH obtained from electronic excitation of IPN at 193 nm.

a primary decomposition product from NM and IPN, but not DMNA, at 193 nm excitation. The NO_2 product in the 1^2B_2 excited state can dissociate into NO (X) and O (^3P) as secondary dissociation products. This NO product is observed in state resolved detection through TOFMS.

B. HONO elimination channel

The HONO elimination channel will eventually produce OH and NO as decomposition products. In order to probe the HONO elimination channel for decomposition of electronically excited NM, DMNA, and IPN, LIF detection of the OH radical is therefore undertaken. The OH product from the photolysis of these three molecules is detected by LIF spectroscopy using two laser beams: one laser beam at 226 nm is used to initiate the dissociation, and another at 308 nm is used to excite the OH radical at its $A^2\Sigma(v' = 0) \leftarrow X^2\Pi(v'' = 0)$ vibronic transition. The LIF spectrum of OH from photolysis of IPN is shown in Fig. 4. Spectral simulation based on a Boltzmann population distribution in the rotational energy levels of the $v'' = 0$ state produces rotational temperature of $\sim 1500 \text{ K}$. OH radicals from the decomposition of DMNA and NM at 226 nm are also found to have similar hot ($\sim 1500 \text{ K}$) rotational distributions. Decomposition of NM, DMNA, and IPN at 226 nm generates less than a 2 mV LIF signal for the OH radical at maximum gain of the photomultiplier tube (PMT). Under similar experimental conditions, the maximum LIF signal intensity of the NO product is observed to be 50 mV for DMNA and more than 1 V for NM and IPN at 226 nm excitation. Experimentally, we observe that the signal intensity of NO is much greater than that of OH particularly from NM and IPN. This signal ratio indicates that the HONO elimination channel has only a very minor contribution to the overall decomposition of NM, DMNA, and IPN. Although the HONO elimination channel plays a minor role in the decomposition of all three molecules, it does present a common decomposition pathway for the different X– NO_2 containing species.

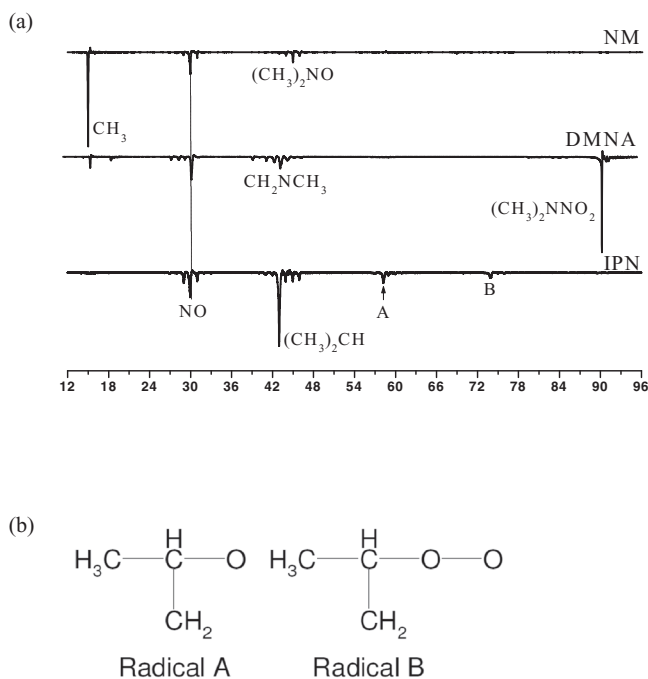


FIG. 5. (a) TOFMS of NM, DMNA, IPN obtained following electronic excitation of the molecules at 193 nm and subsequent ionization of the products at 118 nm. (b) Primary structures of radicals A and B from IPN.

C. Determination of decomposition pathways based on mass spectral analysis

Mass spectra obtained by 193 nm excitation of NM, DMNA, and IPN in the ionization region of a TOFMS with 118 nm ionization of decomposition products, are illustrated in Fig. 5. The primary decomposition channel following 193 nm excitation is suggested to be NO_2 elimination from NM and nitro–nitrite isomerization from DMNA. As illustrated in the mass spectrum of NM (see Fig. 5), the CH_3 mass channel shows much greater intensity than that of the NO mass channel, which is produced from the secondary decomposition of the primary NO_2 product. Another weak peak at mass channel 45 amu is produced by O elimination from NM, which has been discussed in detail in our previous report.⁶ The mass spectrum of DMNA, on the other hand, shows NO, CH_2NCH_3 , and the parent mass features. Using different ns pulsed laser experiments and exploring excited electronic state potential energy surfaces computationally at the CASSCF level of theory, we have previously established that nitro–nitrite isomerization, followed by NO elimination, is the major decomposition channel for electronically excited DMNA.⁷ The NO mass channel feature in the NM mass spectrum is indicative of this isomerization channel.

The mass spectrum for IPN, on the other hand, clearly reveals several important mass peaks corresponding to NO (30 amu), $(\text{CH}_3)_2\text{CH}$ (43 amu), A (58 amu), and B (74 amu). A and B are depicted explicitly in Fig. 5. The most prominent peak at mass channel 43 amu ($(\text{CH}_3)_2\text{CH}$) indicates NO_2 elimination as the major decomposition channel of IPN

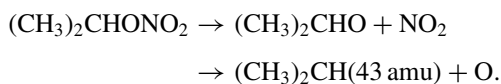


TABLE I. Different decomposition channels observed in the initial decomposition of nitro-containing model systems with mono C– NO_2 , N– NO_2 , and O– NO_2 moieties.

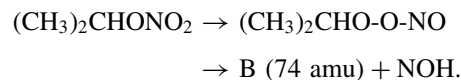
C– NO_2	N– NO_2	O– NO_2
Nitromethane NM	Dimethylnitramine DMNA	Isopropylnitrate IPN
Major		
NO_2 elimination	Nitro–nitrite isomerization	NO_2 elimination
Minor		
HONO elimination	HONO elimination	HONO elimination
O-elimination		Nitro–nitrite isomerization

This $(\text{CH}_3)_2\text{CH}$ radical might also arise from an NO_3 elimination pathway; however, we exclude this possibility for two reasons: observation of fluorescence emission from excited state NO_2 in the visible region upon photolysis of IPN at 193 nm, and similar rotational and vibrational distributions of the NO product from IPN and NM, for which NO_2 elimination is observed to be the major decomposition channel.

Observation of radical A at 58 amu with minor intensity infers again the minor contribution of the HONO elimination channel



Direct observation of weak intensity of radical B at mass channel 74 amu indicates that the nitro–nitrite isomerization mechanism also has minor contribution to the overall decomposition of electronically excited IPN.



Therefore, based on the experimental observations discussed above, we can draw the conclusions that the decomposition of electronically excited NM is mainly governed by the NO_2 elimination mechanism with minor contributions from HONO and O elimination channels. The decomposition of electronically excited IPN is also governed by NO_2 elimination with minor contributions from HONO elimination and nitro–nitrite isomerization mechanisms. The decomposition of electronically excited DMNA, however, is primarily governed by nitro–nitrite isomerization with minor contribution from HONO elimination. For comparison, different decomposition channels observed for X– NO_2 systems studied here are summarized in Table I.

IV. THEORETICAL RESULTS

Detailed analysis of the experimental results indicates that the NO_2 elimination mechanism is the primary decomposition pathway of electronically excited NM (with C– NO_2 moiety) and IPN (with O– NO_2 moiety); however, the nitro–nitrite isomerization mechanism is the major decomposition pathway of DMNA (N– NO_2 moiety). The theoretical model for the decomposition of electronically excited NM (Ref. 9) and DMNA (Ref. 7) has been previously reported in literature. The theoretical model for the decomposition of electronically excited IPN has, however, not been explored thus

TABLE II. Vertical excitation energies (E_{vert}) and relative energies of different critical points of IPN with respect to its ground state FC energy.

State/CI/TS/Min	Configuration	ΔE (eV)
$S_{1,\text{FC}}$	$(n\sigma_{\text{O}},\pi^*)$	5.22
$S_{2,\text{FC}}$	(π,π^*)	6.30
S_1 , O–NO ₂ dissociation	...	4.96
$(S_2/S_1)_{\text{CI}}$...	4.20
$S_{1,\text{Min}}$...	3.76

far. In the present work, excited electronic state PESs of IPN, particularly along the O–NO₂ bond dissociation pathway, explored at CASSCF(10,7)/6-31G(d) level of theory, are presented and contrasted with excited electronic state PESs of NM and DMNA.

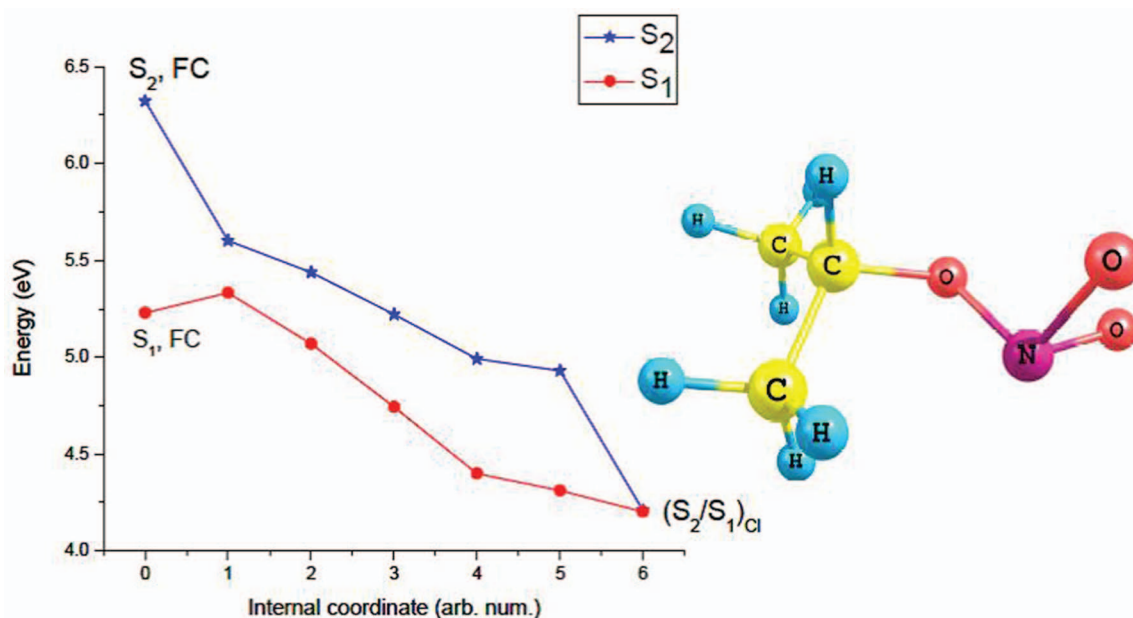
The vertical excitation energies (E_{vert}) for IPN, computed at the CASSCF(10,7)/6-31G(d) optimized Franck-Condon geometry (FC geometry at ground state minimum) are listed in Table II. The calculations show that the two lowest lying excited electronic states (S_1 and S_2) for IPN possess vertical excitation energies of 5.22 and 6.30 eV, respectively: S_1 and S_2 states are of (n,π^*) and (π,π^*) character, respectively. Experimentally, gas phase IPN exhibits a broad, unstructured UV absorption spectrum.⁸ An intense band centered in the 190–220 nm wavelength region results from a (π,π^*) transition, and a weaker band, assigned to as an (n,π^*) excitation, appears as a longer wavelength shoulder that extends as far as 330 nm. The calculated vertical excitation energy of the S_2 state of IPN is in approximately good agreement with the intense band centered in the 190–220 nm region. Adiabatic excitation energy for the S_1 state ($E(S_{1,\text{Min}}) - E(S_{0,\text{FC}})$) is calculated to be 3.76 eV, which is in good agreement with the longer-wavelength shoulder which extends to 330 nm.

A number of critical points on the excited state PESs of IPN, such as [conical intersection (CI)] $(S_2/S_1)_{\text{CI}}$, $S_{1,\text{TS}}$ as-

sociated with NO₂ elimination, and $S_{1,\text{Min}}$, are optimized using the GAUSSIAN 09 program.¹⁰ The minimum energy pathways (or steepest decent pathways) connecting the FC points of the S_1 and S_2 states to the $(S_2/S_1)_{\text{CI}}$ are also explicitly calculated at the CAS(10,7)/6-31G(d) level using an intrinsic reaction coordinate algorithm and are depicted in Fig. 6. The decay paths connecting the FC point of the S_2 and S_1 states to an $(S_2/S_1)_{\text{CI}}$ conical intersection on the S_2 and S_1 surfaces, respectively, are calculated to be barrierless. Fig. 6 also shows the geometry of IPN at the $(S_2/S_1)_{\text{CI}}$ CI, including a bent structure for the O–NO₂ moiety. Fig. 7 shows the decay path from the S_1 FC point to the minimum of the S_1 state ($S_{1,\text{Min}}$): this path is also predicted to be barrierless at the CAS(10,7)/6-31G(d) level of theory. Geometry at $S_{1,\text{Min}}$ shows a bent structure for the O–NO₂ moiety. Fig. 8 shows a PES scan from $S_{1,\text{Min}}$ along the NO₂ elimination path on the S_1 surface. The NO₂ moiety adopts a linear geometry when the O–NO₂ bond distance becomes ~ 3 Å and above. A linear geometry for NO₂ is indicative of excited state NO₂ (1^2B_2) product because electronic ground state NO₂ has a bent geometry with an ONO bond angle of 140°. NO₂ elimination on the S_1 surface is predicted to possess an activation energy barrier of 1.2 eV with respect to the $S_{1,\text{Min}}$.

V. DISCUSSION AND CONCLUSIONS

A schematic one-dimensional plot of the multidimensional singlet PESs (S_0 , S_1 , and S_2) of IPN along the minimum energy (steepest decent) paths with locations and structures of two important critical points on the O–NO₂ bond dissociation reaction coordinate is depicted in Fig. 9. This schematic one dimensional plot of PESs of IPN is drawn based on Figs. 5–7 to provide a concise description of all nonadiabatically coupled electronic PESs of IPN together. Comparison of the excitation energies (5.5 eV at 226 nm, 5.26 eV at 236 nm, 6.4 eV at 193 nm) used in the present photofragmentation-fragment detection experimental

FIG. 6. Minimum energy path connecting FC points of the S_1 and S_2 states to the $(S_2/S_1)_{\text{CI}}$ of IPN.

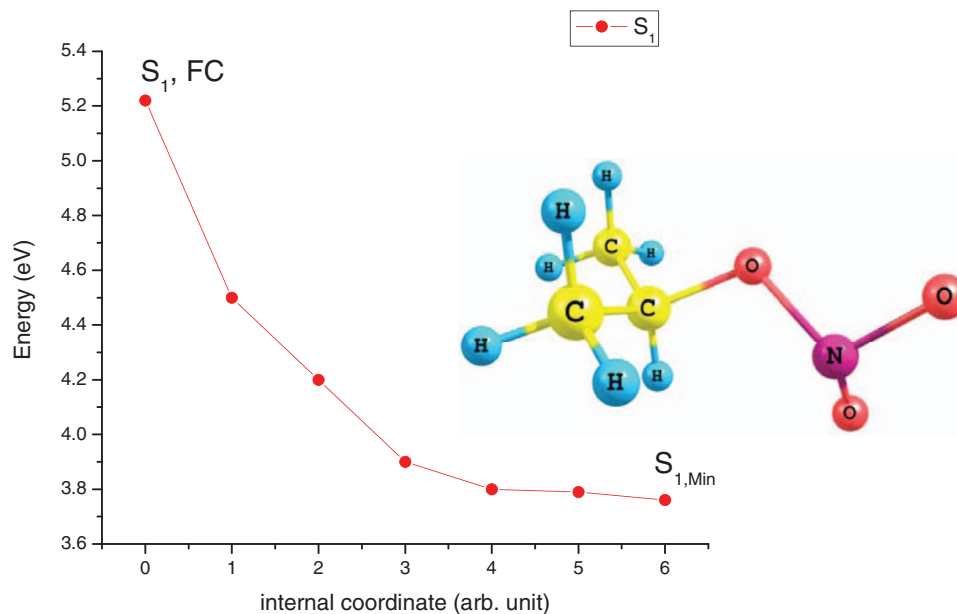
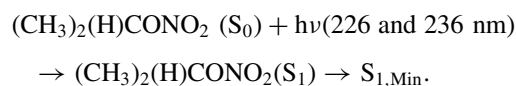
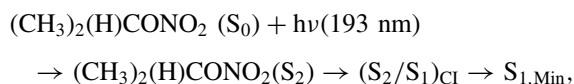


FIG. 7. Minimum energy path connecting the FC point on the S_1 PES to the S_1 minimum for IPN.

work, with the calculated vertical excitation energies at the CASSCF(10,7)/6-31G(d) level, indicates that these UV photoexcitations of IPN primarily populate either the lower vibrational manifolds of the S_2 surface or the upper vibrational manifolds of the S_1 surface. Fig. 9 shows that, following vertical excitation of IPN to even its lower vibronic manifold of the S_2 surface near 193 nm (6.4 eV), the molecule can undergo rapid nonadiabatic internal conversion from S_2 to S_1 through the $(S_2/S_1)_{CI}$ CI. Electronic excitation at 226 nm (5.5 eV) and 236 nm (5.26 eV), on the other hand, promotes the molecule to the S_1 state



Thereafter, the molecule can undergo NO_2 elimination on the S_1 surface, generating excited state NO_2 (1^2B_2).



In order to undergo NO_2 elimination on the S_1 surface, the molecule must surmount an activation energy barrier of 4.96 eV with respect to the ground state FC point, which is accessible with the three photon energies (5.5, 5.26, and 6.4 eV) used in the present experiment. Thus the above model is in good agreement with the experimental observations for IPN,

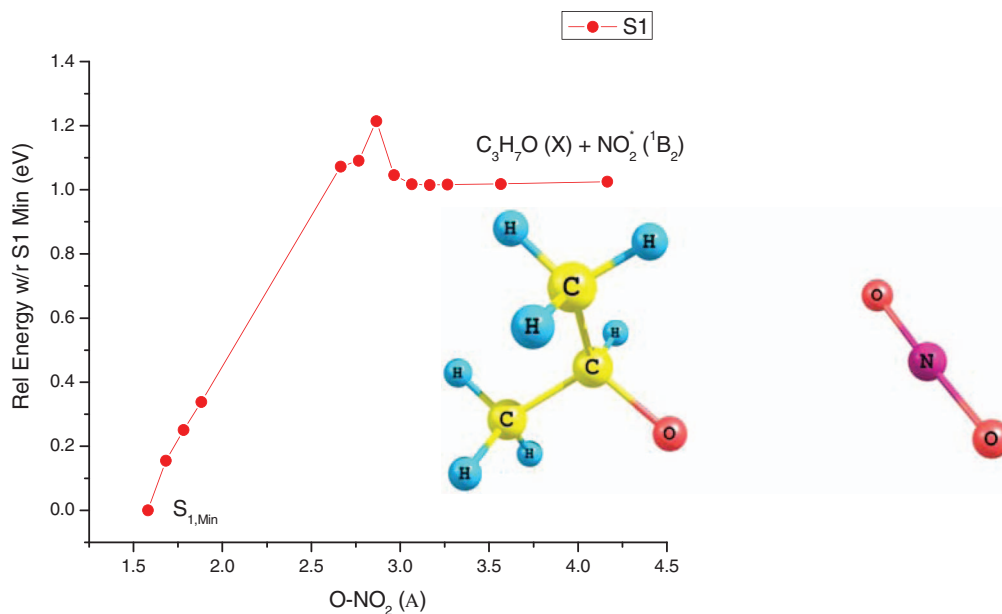


FIG. 8. Minimum energy path for NO_2 elimination of IPN on the S_1 state.

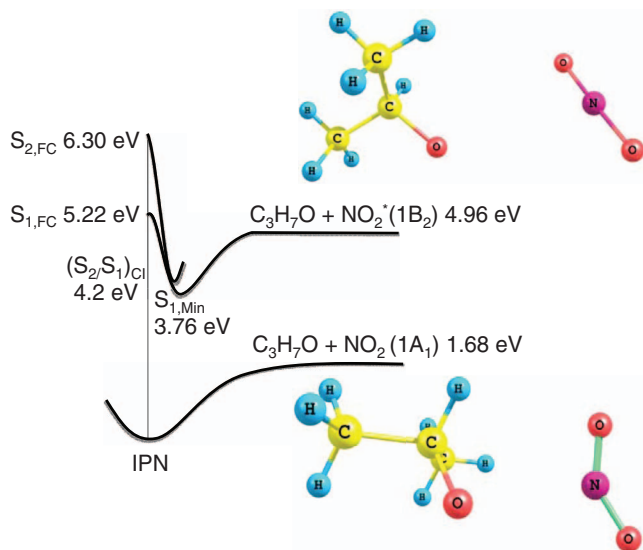
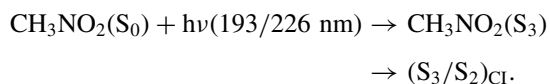


FIG. 9. Schematic one dimensional plot of excited electronic state PESs of IPN.

which suggests that NO_2 elimination is the major decomposition channel of IPN yielding an excited state NO_2 product.

Calculations for the excited state PESs of NM have been performed at CASPT2/ANO-L level of theory by Soto *et al.*,⁹ which are in good agreement with our previous experimental results.⁶ For comparison, the energies of different excited states and conical intersections on the excited electronic state potential energy surfaces of NM are depicted in Fig. 10, which reveals that the key mechanistic step in the decomposition of NM following electronic excitation at 193/226 nm begins with a radiationless internal conversion to the S_2 surface,



Thereafter, the following reaction pathways are accessible:

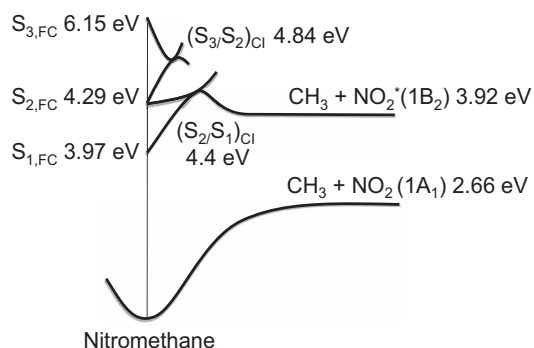
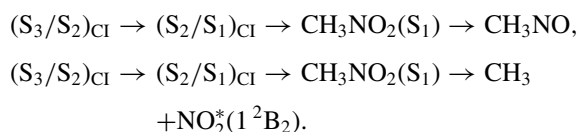


FIG. 10. Nitromethane energy profile, calculated at a CASPT2 theory level by Soto *et al.* (Ref. 9).

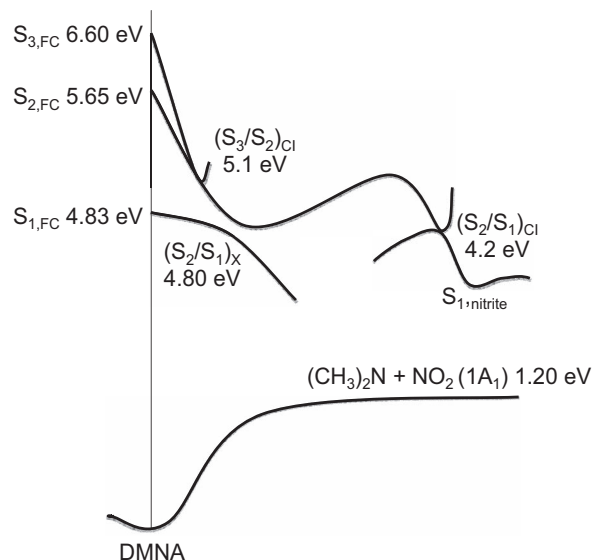
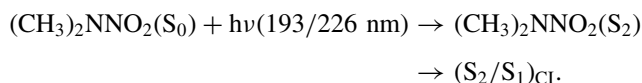


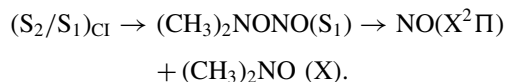
FIG. 11. Energy profile for DMNA calculated at the CASSCF/6-31G(d) level of theory.

NO_2 product in the 1^2B_2 state can subsequently further decompose into $\text{NO}(X^2\Pi) + \text{O}(^3\text{P})$ provided that NO_2 is generated vibrationally hot on the respective electronic surface.

One-dimensional projection of the multidimensional electronic potential energy surfaces of DMNA computed at the CASSCF(10,7)/6-31G(d) level of theory is also reported previously in literature and is shown in Fig. 11. This plot reveals that the key mechanistic step in the decomposition of DMNA following electronic excitation at 193/226 nm is radiationless decay through the $(S_2/S_1)_{\text{CI}}$



Geometry at $(S_2/S_1)_{\text{CI}}$ corresponds to a transition state geometry for nitro–nitrite isomerization. Thereafter, the following reaction pathway becomes accessible for DMNA:



The theoretical decomposition models discussed above for NM, DMNA, and IPN, which are in good agreement with the respective experimental observations, differ mechanistically from one another. Electronically excited DMNA mostly isomerizes, whereas electronically excited NM and IPN certainly do not. The reason for this different mechanistic behavior can be understood by comparing the excited electronic state PESs of DMNA and NM or IPN. Presence of a conical intersection in the nitro–nitrite isomerization reaction coordinate of electronically excited DMNA, which is absent in the same coordinate of NM and IPN, causes a topological alteration of the potential energy surfaces providing a direct nonadiabatic pathway for excited state isomerization of DMNA and eventual elimination of NO . The reason for the different mechanistic behavior also lies in the difference in electronic properties of nitroalkane ($\text{C}-\text{NO}_2$), nitramine ($\text{N}-\text{NO}_2$), and nitro esters ($\text{O}-\text{NO}_2$) active moieties. Presence of different numbers of lone pair electrons on the X atoms and their different

electronegativities produce different electrostatic potential influence on the X–NO₂ (X = N and O) moieties. In a broader sense, thus, present work shows that the energetic behavior of all nitro-containing energetic species may not be similar, and that their energetic behavior can be controlled by specific X–NO₂ bond connectivities.

Furthermore, decomposition of all nitro-containing model systems such as NM, DMNA, and IPN occurs on the S₁ excited state. They all possess a single X–NO₂ energetic moiety; however, high density energetic materials such as TNT, RDX, and PETN all possess more than one X–NO₂ moiety (see Fig. 1) and they decompose on their ground electronic state PESs following nonadiabatic internal conversion to the ground state from upper electronic states.^{7,5} Therefore, the energetic behavior of nitro containing species is controlled not only by specific X–NO₂ bond connectivity, as anticipated from present study, but also by number of X–NO₂ energetic moieties present in the molecule. Further systematic investigations in the direction followed in this research are required to generate a deeper understanding of the molecular decomposition behavior of energetic materials with multiple NO₂ moieties. Nonetheless, one point is clear and essential in the search for general systematics for the comparative chemistry of energetic materials and their model systems: the explication of their different chemistry lies within the details of the nonadiabatic electronic state behavior and the energetics of the conical intersections thereby created. Note, that all energetic materials that we have explored thus far undergo a nonadiabatic conversion of electronic excitation energy into ground electronic state vibrational energy prior to entering the initial reaction channel for decomposition.

ACKNOWLEDGMENTS

This work is supported by Army Research Office (ARO) under Contract No. W911NF-10-1-0117 P00001. Theoretic-

cal calculations were performed at Teragrid Super Computer Center supported by the National Science Foundation (NSF) under Grant No. TG-CHE090094.

- ¹E. R. Bernstein, *Overviews of Recent Research on Energetic Materials*, edited by D. Thompson, T. Brill, and R. Shaw (World Scientific, New Jersey, 2004); F. E. Williams, *Adv. Chem. Phys.* **21**, 289 (1971); J. Sharma, B. C. Beard, and M. Chaykovsky, *J. Phys. Chem.* **95**, 1209 (1991); J. Gilman, *Philos. Mag. B*, **71**, 1057 (1995); M. M. Kuklja, B. P. Aduiev, E. D. Aluker, V. I. Krasheninina, A. G. Krechetov, and A. Y. Mitrofanov, *J. Appl. Phys.* **89**, 4156 (2001); H. M. Windawi, S. P. Varma, C. B. Cooper, and F. Williams, *ibid.* **47**, 3418 (1976); J. Schanda, B. Baron, and F. Williams, *ibid.* **80**, 185 (1975); J. Schanda, B. Baron, and F. Williams, *J. Lumin.* **9**, 338 (1974); S. P. Varma and F. Williams, *J. Chem. Phys.* **59**, 912 (1973); R. B. Hall and F. Williams, *ibid.* **58**, 1036 (1973); F. Williams, *Adv. Chem. Phys.* **21**, 289 (1971); J. Sharma, J. W. Forbes, C. S. Coffey, and T. Liddiard, *J. Phys. Chem.* **91**, 5139 (1987); J. Sharma, and B. C. Beard, in *Structures and Properties of Energetic Materials*, edited by D. H. Lidenberg, R. W. Armstrong, and J. J. Gilman (Mater. Res. Soc. Symp. Proc., Pittsburgh, Pennsylvania, 1993).
- ²J. J. Gilman, *Chem. Propulsion Inf. Agency* **589**, 379 (1992).
- ³B. P. Aduiev, E. D. Aluker, G. M. Belokurov, and A. G. Krechetov, *Chem. Phys. Rep.* **16**, 1479 (1997).
- ⁴A. B. Kunz, M. M. Kuklja, T. R. Botcher, and T. P. Russell, *Thermochim. Acta* **384**, 279 (2002).
- ⁵M. Greenfield, Y. Q. Guo, and E. R. Bernstein, *Chem. Phys. Lett.* **430**, 277 (2006); A. Bhattacharya and E. R. Bernstein, *J. Phys. Chem. A* **115**, 4135 (2011).
- ⁶Y. Q. Guo, A. Bhattacharya, and E. R. Bernstein, *J. Phys. Chem. A* **113**, 85 (2009).
- ⁷A. Bhattacharya, Y. Q. Guo, and E. R. Bernstein, *J. Phys. Chem. A* **113**, 811 (2009); *Acc. Chem. Res.* **43**, 1476 (2010).
- ⁸E. W. R. Steacie and G. T. Shaw, *Proc. R. Soc. London Ser. A* **151**, 685 (1935); P. G. Carbajo and A. J. Orr-Ewing, *Phys. Chem. Chem. Phys.* **12**, 6084 (2010); R. J. Talukdar, J. B. Burkholder, M. Hunter, M. K. Gilles, J. M. Roberts, and A. R. Ravishankara, *J. Chem. Soc., Faraday Trans.* **93**, 2797 (1997).
- ⁹J. F. Arenas, J. C. Otero, D. Pelaez, and J. Soto, *J. Chem. Phys.* **119**, 7814 (2003); **122**, 084324 (2005).
- ¹⁰M. J. Frisch, G. W. Trucks, H. B. Schlegel, *et al.*, GAUSSIAN 03, Revision B.04, Gaussian, Inc., Pittsburgh, PA, 2003.
- ¹¹L. J. Bultler, D. Krajnovich, and Y. T. Lee, *J. Chem. Phys.* **79**, 1708 (1983).